

UDK 677.017.5

Optoelectronic Properties Correlation to Preparation of Au/La-oxide Nanocomposite Films

A. A. Dakhel

Department of Physics, College of Science, University of Bahrain, P.O. Box 32038, Kingdom of Bahrain

Abstract:

Gold nanoparticles were grown in La-oxide thin films deposited on quartz and silicon substrates. These films were annealed in pure hydrogen gas atmosphere at 300 °C for different durations 15 min, 30 min, and 45 min and characterised by the X-ray fluorescence (XRF) and X-ray diffraction. The matrix La-oxide remained amorphous up to 400 °C. The fraction of Au in La-oxide host material was 7 % molar with crystallite size of 6.8 nm. The Au NPs slightly grew by annealing in H₂ gas at 300 K. The samples were investigated by UV-Vis-NIR absorption spectroscopy and dc-electrical measurements. They exhibit conducting properties and with H₂ gas annealing, they showed red shifting of the bandgap with remarkable reduction of optical absorption coefficient by ~25 % and remarkable increase in electrical conductivity ~124 %. A global study of the influence of low-temperature post annealing in H₂ gas on the electrical, structural, optical, and optoelectronic properties was conducted.

Keywords: Optical properties; Au-incorporated La oxide; Composite materials; Annealing in H₂ gas, Gold plasmon.

1. Introduction

Composites including ceramics and cermets have various applications in different industrial fields. Such obtained nanocomposite materials has enabled obtaining exceptional effects of a good, for example, combination of mechanical -electric properties [1]. For instance, electrical components can get very hot, they need to behave like ceramics, but, since they also need to conduct electricity, it helps if they work like metals. Cermets are suitable to use in components such as resistors. Various oxides and ceramics that include metallic nanoparticles (NPs) have received much attention for their unique optical properties, which found a variety of applications as optical diodes, chemical gas sensors, etc [2-7] as well as used in transparent conducting oxide (TCO) applications [8-11]. For example, Au-incorporated ZnO nanomaterial was successfully used as sensor (electronic nose) for detection of volatile organic compounds [12]. Recently, gold NPs of sizes 3-6 nm supported on rare-earth oxide medium with a concentration of 1-2 %mol was prepared by chemical method and morphologically investigated [13]. The present work reports the optical and conduction properties of conductive gold NPs-incorporated lanthanum oxide films post-annealed in hydrogen atmosphere for different optical and electrical applications.

It was found experimentally that the low-temperature post-annealing in H₂ gas

*) **Corresponding author:** adakhil@sci.uob.bh

(without reduction) enhances the electrical conduction of many metal oxides like CdO, SnO₂, ZnO, and Al-doped ZnO [14-17]. This conduction enhancement was attributed to the reducing in the effect of depletion regions formed on grain and crystallite boundaries [17-19] rather than creation of H⁺ ions in the lattice of annealed oxide as was explained in Ref [20-22]. The present work investigates this point i.e. investigate the enhancement of electrical conduction of La-oxide films incorporated with Au NPs by annealing in H₂ gas and its influence on the structural and optical properties.

2. Experimental details

The starting materials were pure lanthanum element 99.9 % (from Fluka A. G.) and pure gold metal 99.99 % (from Aldrich Chem. Co.). The alternating thermal deposition (layer-by-layer, etc) method was used to deposit the starting materials on clean quartz (from SPI supplies, PA, USA) and silicon wafer substrates held at about 150 °C in a vacuum chamber of residual oxygen atmosphere of pressure about 1.3×10^{-2} Pa. The evaporated masses were controlled with a piezoelectric microbalance crystal sensor (Philips FTM5) fixed close to the substrates. The as-grown films were totally oxidised and stabilised by flash annealing in pure dry O₂-atmosphere at 400 °C for 1 h. The final film's thickness was measured after annealing by Gaertner L117 ellipsometer. The molar ratio (r) of Au relative to La were determined by energy dispersive X-ray fluorescence (EDX) technique using a setup with an X-ray beam obtained from a Cu-anode Philips tube (Philips PW-1710) operating at regime 15 kV, 5 mA, and an Amptek XR-100CR sensitive detector. The radiographic analysis method [23, 24] was used to determine r. It based on measuring of the integral intensity of La L α signal excited by Cu K α -line and Au L α signal excited by the bremsstrahlung radiation. The reference samples were pure thin La₂O₃ and Au films. The structures of the films were studied by θ -2 θ X-ray diffraction (XRD) method using a Philips PW 1710 with Cu K α radiation (0.15406 nm) and step 0.01°. The spectral optical transmittance and reflectance were measured at normal incidence in UV-VIS-NIR spectral region (300-3000 nm) with a Shimadzu UV-3600 double beam spectrophotometer. The resistivity was measured by conventional two-lead method.

One set of films of 5%Au (molar) were found to be insulating of resistivity about $9.6 \times 10^4 \Omega \cdot cm$, which is lower than that of identically prepared pure La oxide of about $3.1 \times 10^7 \Omega \cdot cm$ [25]. However, second set of films of 7%Au were found to be conducting of resistivity about $1.6 \times 10^{-3} \Omega \cdot cm$ and TCC of $1.2 \times 10^{-3} K^{-1}$. This means that the electronic percolation threshold (EPT) should be around 6 % (in-between 5 % and 7 %molar). The variation of the resistivity is given in semilog graph as inset of Fig.2. The set of conductive films of 7%Au were further processed by annealing in hydrogen atmosphere at 300 °C for 15 min (H15), 30 min (H30), and 45 min (H45) (H0 refers to the non-hydrogenated Au/La-oxide composite film).

3. Results and discussions

Fig. 1. shows the XRD patterns of Au/La-oxide nanocomposite samples (H0, H15, H30, and H45) with that of a pure La-oxide film grown on quartz substrates. The patterns reveal that La oxide, as medium for growth of Au NPs, is amorphous for all studied samples. Thus, the prepared Au/La-oxide films consist of Au NPs of mean X-ray NPs size (D) about 6.8 nm (estimated by using Scherrer's relation [24] with a Gaussian peak fitting) embedded in amorphous La-oxide medium. It must be mentioned here that according to our previous studies on La-oxide film prepared by the same procedure [26], the oxide crystallises mainly in

trigonal structure La_2O_3 when annealed at 600 °C. The intense (111) peak of Au NPs is shifted as compared with that of pure Au due to the structural strain that was calculated and given in Table I with its corresponding compressive strain (the estimation was done by using the bulk modulus (B) given in ref.[27]). From Tab. I, one can observe that annealing in H_2 gas gradually removed the structural stress reaching minimum value in H15 film, and then approached a steady state value in H30 and H45 films.

Tab. I Au (111) X-ray reflection Bragg angle, $2\theta_{111}^\circ$; average Au crystallite size, D (nm); compressive structural strain of Au NPs, $\varepsilon_s (\times 10^{-3})$; compressive stress on Au NPs, σ_{st} (GPa); bandgap, E_g (eV); reflection threshold energy, $\hbar\omega_{\min}$ (eV); resistivity, $\rho (\times 10^{-1} \Omega \text{cm})$; concentration of electrons, $N_{el} (\times 10^{18} \text{cm}^{-3})$; carrier mobility, and $\mu (\text{cm}^2/\text{V.s})$ of the prepared H0, H15, H30, H45, Au/La-oxide nanocomposite films grown on quartz substrates.

Sample	$2\theta_{111}^\circ$	D(nm)	ε_s	σ_{st}	E_g	$\hbar\omega_{\min}$	ρ	N_{el}	μ
H0	38.66	6.8	12.4	2.15	5.91	1.165	18.4	4.93	0.69
H15	38.24	7.8	2.0	0.35	5.55	1.095	8.2	4.35	1.75
H30	38.36	8.2	5.0	0.87	5.66	1.099	9.8	4.38	1.45
H45	38.36	8.1	5.0	0.87	5.66	1.114	9.8	4.51	1.42

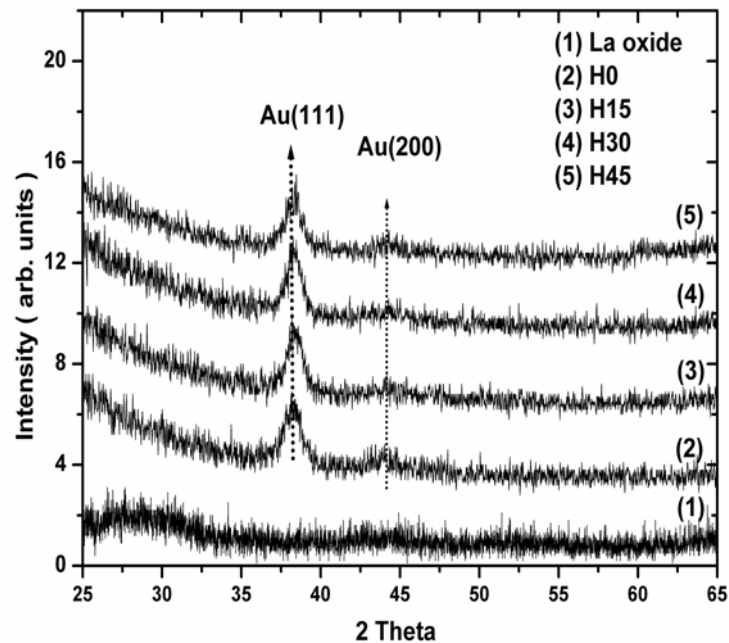


Fig. 1. XRD patterns of H0, H15, H30, and H45 films together with that of a pure La oxide film grown on quartz substrates. The radiation used was $\text{Cu K}\alpha$ - line.

The 7 %Au/La-oxide nanocomposite film resistivity as a function of time duration of post annealing in H_2 gas atmosphere is presented in Fig. 2. The hydrogenated samples have almost same TCC as that of non-hydrogenated sample. As seen, the conductivity of the films was improved with H_2 -annealing.

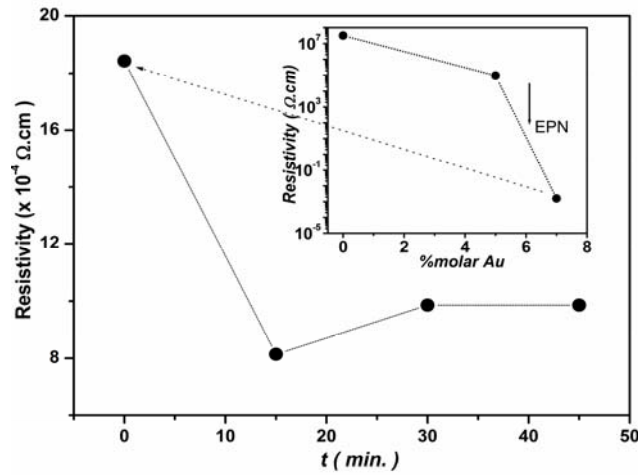


Fig. 2. Dependence of resistivity of Au/La-oxide nanocomposite film on the time of annealing in pure H_2 gas atmosphere. The inset shows the variation of resistivity on % molar Au content in Au/La-oxide nanocomposite film showing the I-to-M transformation near $\sim 6\%$.

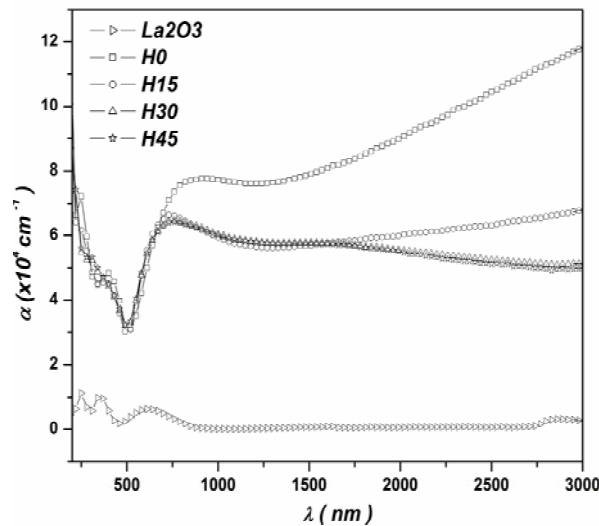


Fig. 3. Normal spectral absorption coefficient in the UV-Vis-NIR regions for H0, H15, H30, and H45 films together with that of pure La oxide grown on quartz substrates.

The spectral absorption coefficient $\alpha(\lambda)$ was calculated from the experimental data of normal transmittance $T(\lambda)$ and reflectance $R(\lambda)$ by [28]: $\alpha(\lambda) = (1/d) \ln[(1-R)/T]$, where d is the film thickness; $0.175 \mu m$ for 7% Au film and $0.24 \mu m$ for La-oxide film. The experimental data of $R(\lambda)$ and $T(\lambda)$ were corrected due to the substrate effects according to the method given in Ref. [29], which needs to measure the reflectance from both sides of the film/substrate system. Fig.3. shows the spectral absorption coefficient $\alpha(\lambda)$ in the UV-Vis-NIR wavelength range for H0, H15, H30, and H45 films together with that of La-Oxide film grown on quartz substrates. A clear effect of annealing in H_2 gas appears in Vis and NIR regions was observed, where both the transmittance and reflectance have increased with time-period of annealing in H_2 gas. The precise investigation showed that the peaks observed on the spectrum are due to the interference phenomenon and the Au surface plasmon resonance (SPR) absorption feature being in the range 500 – 650 nm cannot be separated and studied alone due to the total overlapping. It is important to mention here that Au SPR could be

clearly observed only when the Au grain size ~ 3.5 nm or less [30].

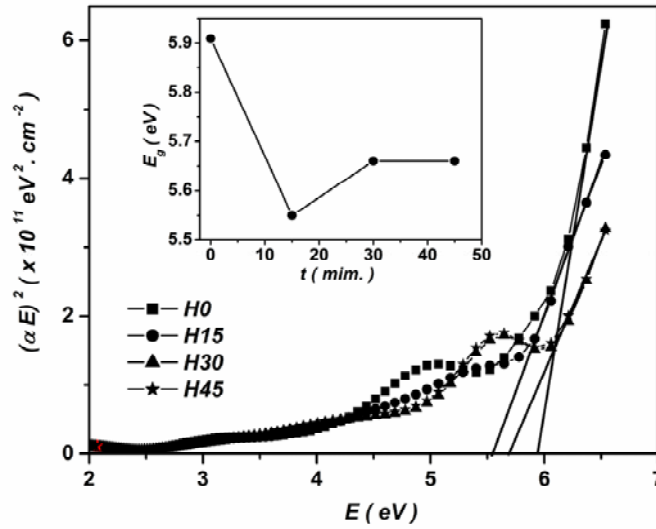


Fig. 4. Tauc plot of $(\alpha E)^2$ vs. photon energy (E) for direct bandgap determination. The inset shows the variation of bandgap with annealing time in H_2 gas atmosphere.

The absorption coefficient is related to the incident photon energy ($E = \hbar\omega$) by: $\alpha E \sim (E - E_g)^m$ [31], where E_g is the band gap of the film material and the exponent m depends on the type of transitions: $m=1/2, 2$ corresponding to the direct and indirect transitions, respectively. It was observed that the best value suitable to the obtained data of the present work is $m=1/2$. Thus, the extrapolating of the linear portion of the $(\alpha E)^2$ vs. E plots to the energy axis, as shown in Fig. 4, give the values of E_g that are tabulated in Table I. The obtained values of E_g for all investigated samples are lower than that of pure La oxide: 6.18 eV [31] or 6.4 eV [32]. It was observed that the energy gap narrowed with low-temperature annealing in H_2 gas, as shown in the inset of Fig. 4, so that the bandgap attains the lowest value for sample H15 (for which the electrical resistivity attains the lowest value and the compression micro stress attains the minimum value.).

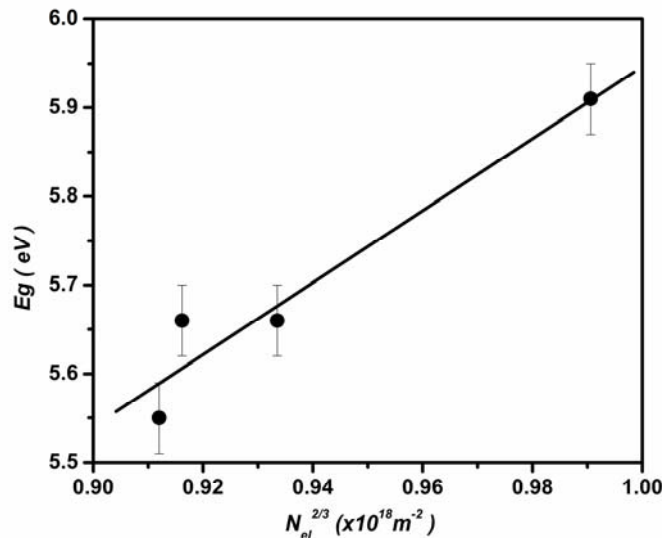


Fig. 5. The dependence of bandgap of H0, H15, H30, and H45 films on $N_{el}^{2/3}$ according to Moss-Burstein effect.

The red shift of principal absorption edge can be interpreted by the effect of Moss-Burstein (B-M). According to B-M model, the optical-absorption edge energy position is proportional to the free-electron density in conduction band (N_{el}) (determined from the reflectance analysis) through the following relation [33,34]: $E_g \sim (\hbar^2 / 2m_{el}^*) (3\pi^2 N_{el})^{2/3}$, where \hbar is the Plank constant, and m_{el}^* the reduced effective mass to free-electron mass. Fig.5 shows the linear relationship E_g vs. $N_{el}^{2/3}$ following B-M model. Analogous results was obtained for the H₂-annealed ZnO:Al and CdO [16,35].

The reflectance spectra, $R(\lambda)$, for H0, H15, H30, and H45 films shown in Fig. 6. have a metal-like behaviour. The reflection is due to the gold nanoparticles. It shows almost linear increasing function of λ in NIR spectral region for $\lambda > 1000$ nm. However, the increasing of R with λ for H30 and H45 films is stronger that that for H0 and H15. For the analysis, the energy dependence of the reflectance in the NIR spectral region was plotted as shown in the inset of Fig. 6.

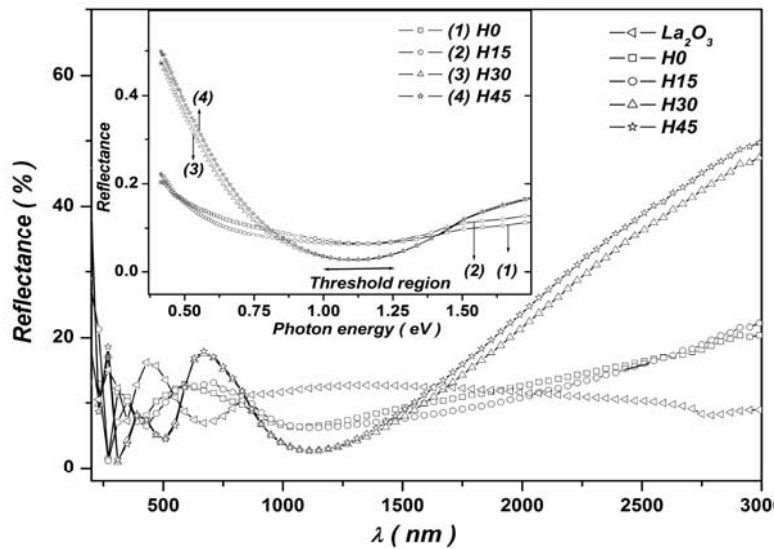


Fig. 6. Normal spectral reflectance in the UV-Vis-NIR regions for H0, H15, H30, and H45 films together with that of pure La oxide grown on quartz substrates. The inset shows the photon-energy dependence of the reflectance in the NIR regions for H0, H15, H30, and H45 films.

The minimum (threshold) of the reflectance spectrum occurs at slightly higher frequency than plasma ω_p , and can be found by $\omega_{min} = \omega_p / (\epsilon_\infty - 1)^{1/2}$ [36], where ϵ_∞ is the dielectric constant for the bound electrons of gold nanoparticles (not the surrounding medium) that caused the reflection behaviour, which is equal to 6.0 [37] or 6.9 [38]. Thus the plasmon energy for H0 is $\hbar\omega_p \approx 2.6 eV$ or $\lambda_p = 478 nm$ which close to the usually found value for gold. The Drude free-electron plasma frequency is defined by [26, 39]: $\omega_p^2 = N_{el} e^2 / m_{el}^* \epsilon_0$, where N_{el} is the electronic concentration, ϵ_0 is the permittivity of free space, and c is the free-space velocity of light. The electronic effective mass m_{el}^* is equal to $(1 \pm 0.03)m_{el}$ in Au, where m_{el} is the free-electron mass [40]. The experimental values of $\hbar\omega_{min}$ for the nanocomposite films are given in Tab. I. The calculated values of N_{el} are given in table I. The carrier mobility

μ_{el} was calculated from the well-known relation $\mu_{el} = (e \rho N_{el})^{-1}$. The carrier concentration as well as the mobility was influenced by the annealing in H_2 gas atmosphere as shown in Fig. 7. In general, one can observe that sample annealed in H_2 for 15 min attain a minimum resistivity of $8.2 \times 10^{-4} \Omega \cdot \text{cm}$, largest mobility $1.75 \text{ cm}^2/\text{V}\cdot\text{s}$, and lowest carrier concentration of $4.35 \times 10^{21} \text{ cm}^{-3}$.

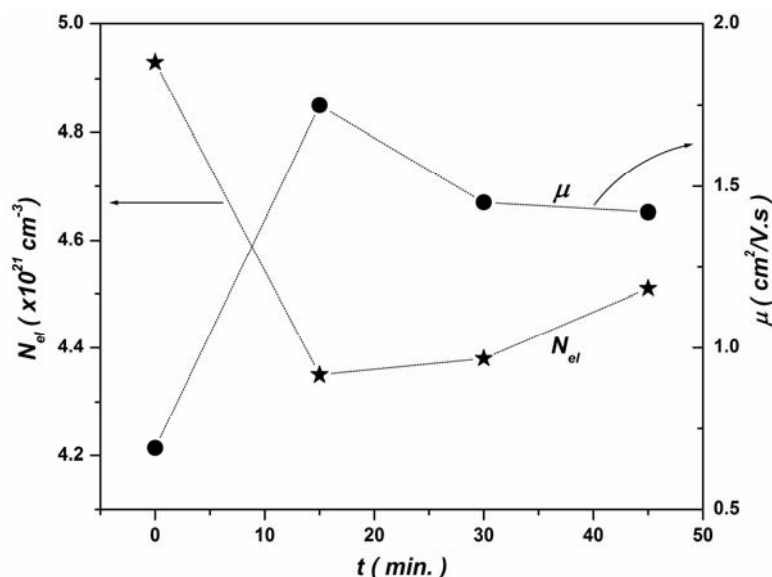


Fig. 7. Dependence of the carrier concentration and mobility of Au/ La-oxide nanocomposite film on the time of annealing in H_2 gas atmosphere.

The electrical conduction in composite systems comprising an intricate network of conducting and insulating phases is determined by two mechanisms, percolation in a continuous conducting network and/or tunneling between isolated conducting particles (grains, crystallites, etc.) [41,43]. For both cases, there is an electronic percolation (EPN) network necessary to conduct electricity by any mechanism including tunneling. This means that the conduction could be controlled by means of annealing in H_2 gas, which affects the physical properties of the electronic conducting network or tunneling network (TN) [43]. In general, one of the favourable roles of annealing in H_2 gas is to reduce or passivity the effect of depletion regions or potential barriers formed between Au grains and, therefore, enhance tunnelling and decreasing the grain boundary scattering, which finally improves the electrical conductivity, as mentioned in Ref.[16,44,45]. Furthermore, the hydrogenation process is related to the increase of electron transfer on Au NPs facilitating through the embedding amorphous medium [46].

4. Conclusions

It was established that La-oxide films incorporated with 7 %Au consist of Au-NPs (6.8 nm) embedded in amorphous La oxide and exhibit conducting properties. Annealing in H_2 gas affects all structural, optical, and electrical properties. It enlarged the Au NPs, reduced the compressive micro stresses on the Au NPs, and reduced the bandgap of the composite film material. Results show that with 15 min annealing in H_2 gas, the transmittance in NIR region increases by about 25 %, the electrical conductivity increases by about 124 %, mobility increases by 153 %, while the carrier concentration was decreased by 12 %. The results show

that the conductivity and mobility have the highest value for H15 sample. The improving of conductivity and optical transmittance of the nanocomposite film under H₂-annealing are important action from TCO application point of view and suggests Au/La-oxide films to be used in TCO-like applications.

5. References

1. Z. Andjic, M. Korac, Z. Kamberovic, A. Vujovic, M. Tasic, *Science of Sintering*, 39 (2007) 145.
2. G. Teowee, K. C. McCarthy, T. J. Bukowski, T. P. Alexander, S. Motakef, D. R. Uhlmann, *Ferroelectrics*, ISAF '96., Proceedings of the Tenth IEEE International Symposium on Applications of, Vol. 2, 1996, pp. 671-674.
3. P. R. Watekar, S. Ju, W. -T. Han, *Colloids and Surfaces A: Physicochem. Eng. Aspects* 313/314 (2008) 492.
4. S. Ju, V. L. Nguyen, P. R. Watekar, B. H. Kim, C. Jeong, S. Boo, W. -T. Han, *J. Nano Sci. Nano Technol.* 6 (2006) 1.
5. M. Menning, M. Schmitt, U. Becker, G. Jung, H. Schmidt, *SPIE Sol-Gel Optics III*, Vol. 2288, pp.130-139,1994.
6. D. Kundu, I. Honma, T. Osawa, H. Komiyama, *J. Am. Ceram. Soc.*, 77 (1994) 1110.
7. S. Ogawa, Y. Hayashi, N. Kobayashi, T. Tokizaki, A. Nakamura, *Jpn. J. Appl. Phys.* 33 (1994) L331.
8. R. Maity, K. K. Chattopadhyay, *Solar Energy Mater. & Solar Cells* 90 (2006) 597.
9. S. Shu, Y. Yang, J. E. Medvedova, J. R. Ireland, A. W. Metz, J. Ni, C. R. Kannewurf, A. J. Freeman, T. J. Tobin, *J. American Chem. Soc.* 126 (2004) 13787.
10. Yu. Yang, S. J. Shu, J. E. Medvedeva, J. R. Ireland, A. W. Metz, Ni Jun, M. C. Hersam, A. J. Freeman, T. J. Marks, *J. Am. Chem. Soc.* 127 (2005) 8796.
11. H. T. Cao, Z. L. Pei, J. Gong, C. Sun, R. F. Huang, L. S. Wen, *Surface Coatings Technol.* 184 (2004) 84.
12. C. Wongchoosuk, S. Choopun, A. Tuantranont, T. Kerdcharoen, *Materials Research Innovations* 13 (2009) 185
13. S. K. Bhargava, D. B. Akolekar, G. Foran, *J. Molecular Catalysis A: Chemical* 267 (2007) 57.
14. G. J. Exarhos, X. -D. Zhou, *Thin Solid Films* 515 (2007) 7025.
15. C. G. Van de Walle, *Phys. Rev. Lett.* 85 (2000) 1012.
16. E. A. Davis, S. F. J. Cox, R. L. Lichti, C. G. Van de Walle, *Appl. Phys. Lett.* 82 (2003) 592.
17. B. Y. Oh, M. C. Jeong, D. S. Kim, W. Lee, J. M. Myoung, *J. Cryst. Growth* 281 (2005) 475.
18. K. Zhang, F. Zhu, C. H. A. Huna, A. T. S. Wee, *J. Appl. Phys.* 86 (1999) 974.
19. S. Y. Myong, K. S. Lim, *Appl. Phys. Lett.* 92 (2003) 3026.
20. C. G. Van de Walle, *J. Alloys Compounds* 446-447 (2007) 48.
21. C. G. Van de Walle, Y. Bar-Yam, S. T. Pantelides, *Phys. Rev. Lett.* 60 (1988) 2761.
22. C. Herring, N. M. Johnson, C. G. Van de Walle, *Phys. Rev. B* 64 (2001) 125209.
23. S. Hayakawa, Jia Xiao-Peng, M. Wakatsuki, Y. Gohshi and T. Hirokawa, *J. Crystal Growth* 210 (2000) 388.
24. E. F. Kaelble(ed.), *Handbook of X-rays for Diffraction, Emission, Absorption, and Microscopy*, McGraw-Hill, New York, 1967, p. 17-5.
25. A. A. Dakhel, *J. Alloys Comp.* 433 (2007) 6-10.
26. A. A. Dakhel, *Mater. Chem. Phys.* 102 (2007) 266.
27. C. Kittel, *Introduction to Solid State Physics*, seventh edition, John Wiley & Sons, Inc., New York, 1996, P.59 and P.273.

28. W. Q. Hong, J. Phys. D: Appl. Phys. 22 (1989) 1384.
29. M. Medles, N. Benramdane, A. Bouzidi, A. Nakrela, H. Tabet-Derraz, Z. Kebbab, C. Mathieu, B. Khelifa, R. Deafeux, Thin Solid films 497 (2006) 58.
30. J. Siegel, O. Lyutakov, V. Rybka, Z. Kolska, V. Svorcık, Nanoscale Research Letters 6 (2011) 96
31. J. Tauc, Optical properties of Solids, Edited by F. Abeles. North Holland, 1969.
32. J. -B. Cheng, A. -D. Li, Q. -Y. Shao, H. -Q. Ling, D. Wu, Y. Wang, Y. -J. Bao, M. Wang, Z. -G. Liu, N. -B. Ming, Appl. Surf. Sci. 233 (2004) 91.
33. E. Burstein, Phys. Rev. 93 (1954) 632.
34. T. S. Moss, Proc. Phys. Soc. Lond. B67 (1954) 775.
35. A. A. Dakhel, Semicond. Sci. Technol. 23 (2008) 055017 (6pp)
36. R. E. Kroon, Infrared Physics & Technology 51 (2007) 31
37. X. Wang, K. -ping Chen, M. Zhao, D. D. Nolte, OpticsExpress 18 (2010) 24859.
38. I. N. Shklyarevskii, P. L. Pakhmov, USSR, Optika i Spektroskopiya 34 (1973)163, MIT internet site: <http://www.mit.edu/~6.777/matprops/gold.htm>
39. Z. Qiao, C. Agashe, D. Mergel, Thin Solid Films 496 (2006) 520
40. J. Szczyrbowski, J. Phys. D: Appl. Phys. 19 (1986) 1257.
41. D. Toker, D. Azulay, N. Shimoni, I. Balberg, O. Millo, Phys. Rev. B 68 (2003) 041403(R) (4 pages)
42. P. Sheng, E. K. Sichel, J. I. Gittleman, Phys. Rev. Lett. 40 (1978) 1197.
43. E.K. Sichel, J.I. Gittleman, P. Sheng, Phys. Rev. B 18 (1978) 5712.
44. M. L. Addonizio, A. Antonaia, G. Cantele, C. Privato, Thin Solid Films 349 (1999) 93.
45. T. Tsuji, M. Hirohashi, Appl. Surf. Sci. 157 (2000) 47.
46. S. Pramanik, S. Pal, G. De, J. Mater. Chem. 20 (2010) 9081.

Садржај: Нано-честице злата расле су у La-оксидним танким филмовима депонованим на кварцим или силицијумским супстратима. Ови филмови су каљени у чистој атмосфери водоника на 300 °C 15, 30, и 45 минута и карактерисани рендгенском флуоресценцијом и дифракцијом. Матрица La-оксида остала је аморфна до 400 °C. Фракција Au у La-оксидном материјалу је 7 молских % са величином кристалита од 6,8 nm. Фракција Au је лагано расла каљењем у H₂ на 300 K. Узорци су испитивани UV-Vis-NIR апсорпционом спектроскопијом и *dc*-електричним мерењима. Показују проводна својства и са каљењем у атмосфери H₂, показују црвено померање енергетске баријере са значајном редуцијом оптичког апсорпционог коефицијента за ~25 % и значајан пораст електричне проводљивости за ~124 %. У раду је приказана општа студија о утицају ниско-температурског каљења у атмосфери H₂ на електрична, структурна, оптичка и оптоелектронска својства.

Кључне речи: оптичка својства; оксид La са инкорпорираним Au; композитни материјали; каљење у гасу H₂, златни плазмон
